Research Square

Preprints are preliminary reports that have not undergone peer review.
They should not be considered conclusive, used to inform clinical practice,
or referenced by the media as validated information.

A Comparative First Principles Study of Two-Dimensional Transition Metal Dichalcogenides

Aylin YILDIZ TUNALI
Dokuz Eylül University
Nazli BOZ YURDASAN
nazli.boz@deu.edu.tr

Dokuz Eylül University
Gonul BILGEC AKYUZ
Aydın Adnan Menderes University

Research Article

Keywords: transition metal dichalcogenides, first-principles calculations, two-dimensional materials, phonon dispersion, Debye temperature

Posted Date: December 20th, 2023

DOI: https://doi.org/10.21203/rs.3.rs-3758497/v1

License: This work is licensed under a Creative Commons Attribution 4.0 International License. Read Full License

Additional Declarations: No competing interests reported.

Version of Record: A version of this preprint was published at Journal of Superconductivity and Novel Magnetism on March 6th, 2024. See the published version at https://doi.org/10.1007/s10948-024-06710-z.

Abstract

In recent years, studies on the two-dimensional transition metal dichalcogenides have become important since their potentials have useful properties in technological applications. In this respect, the structural, electronic and vibrational properties of the 12 transition metal dichalcogenide (TMD) MX_2 (M = Mo,W,Cr,Ni; X = S,Se,Te) sheets are investigated using first-principles calculations. The calculated band structures show that all TMDs are semiconductors with a direct band gap at the K point, except NiX_2 ones with indirect band gaps. We find energetic and dynamical stabilities of the MX_2 sheets, while $NiSe_2$ lattice becomes unstable with negative frequencies appearing in acoustic modes near the K point. We also discuss the role of average atomic mass and interatomic bonding in determining the Debye temperatures of dynamically stable dichalcogenide sheets.

1. Introduction

The first experimental realization of graphene led to intensified research on two-dimensional materials [1, 2, 3]. However, the zero band gap of graphene restricts the various technological applications. Therefore, two dimensional materials, especially mono layer transition metal dichalcogenides (TMDs) have become the focus. Recent studies show that two-dimensional materials are preferred in the production of two-dimensional devices due to their electronic properties [4–8].

The TMD materials are generally in the form of honeycomb with chemical formula MX_2, where M and X denote transitional metal and chalcogen (S, Se, Te) atoms respectively. The structures of the TMDs are characterized by two types: one is the D6h point group symmetry, which is a honeycomb (2H) structure and the other one is D3d point group symmetry, which is a centered honeycomb (1T) structure. These structures could be thought of as a positively charge two-dimensional (2D) hexagonal lattice consisting of M atoms sandwiched between two hexagonal lattices of negatively charged X atoms.

In an experimental study [9], it is reported the liquid exfoliation of some nanosheets (MoS2, WS2, MoSe2, TaSe2, NbSe2, NiTe2 and MoT2) having honeycomblike structures. Additionally, theoretical studies have been achieved on the structural stability, electronic properties and intriguing potential applications on the TMD materials. For instance, Ataca et al. conducted a systematic study on the 88 different combinations of MX_2 compounds [10]. Similarly, the reference [11] presents the electronic structure of semiconducting monolayer TMDs and –oxides in the 2H and 1T hexagonal phases using a comprehensive first-principles study. Y. Ding et al. [12] have also investigated the structural, electronic and vibrational properties of graphene-like TMD sheets using GGA and LDA functionals in the DFT method as implemented in the VASP simulation code. They reported improved direct band gaps of semiconducting MoX_2 and WX_2 dichalcogenides by using GW the technique, while NbX_2 and TaX_2 sheets were found as metals. Research on mechanical, vibrational, and lattice thermal properties of monolayer 1H; Cr, Mo and W dichalcogenides and oxides based on quasi harmonic approximation using first principles calculations has been presented in Ref. [13].

Although many theoretical and experimental studies have been carried out on TMDs structures, studies on physical properties such as Debye temperatures and dynamic behaviors are still insufficient. In this study, we explore the structural, electronic and vibrational properties of 12 different stable 2D single layer MX_2 structures (M = Mo,W,Cr,Ni; X = S,Se,Te) by using the first-principles calculation based on density functional theory (DFT). In addition, the Debye temperatures have been calculated for dynamically stable TMDs by using individual acoustic modes in a simple formula. The calculation methods are given in Section 2 and the obtained results are shown and discussed in Section 3. Our studies provide us a better understanding of the new properties of corresponding TMDs and bring out interesting results that enhance the importance of TMDs in future nanotechnology devices.

2. Computational Methods

First principles calculations have been performed within the framework of density functional theory [14–15] as applied in the Quantum Espresso [16]. All structures are treated using periodic boundary conditions and local density approximation (LDA) is used for the exchangecorrelation potential [17]. To ensure the calculation accuracy, convergence analysis is performed on kinetic energy cut-off and the number of k points. The minimum E_{cut} energy used in our calculations is 1224 eV. Brillouin zone has been performed on the k-point mesh by using the Monkhorst-Pack method. 10x10x1 and 9x9x1 special k-point mesh are generated for MoS_2, WS_2, CrS_2, WSe_2, $CrSe_2$, WTe_2 and $MoSe_2$, $MoTe_2$ structures, respectively. During the structural optimizations, atomic coordinates are relaxed with a tolerance of 10^{-6} Ry in the total energy between two consecutive selfconsistent steps and a force convergence of $4x10^{-4}$ Ry/Bohr using a modified Broyden-Fletcher-Goldfarb-Shanno (BFGS) minimization algorithm. The pressure in the unit cell has been kept less than 1 kbar. Phonon dispersions are computed using the formalism of density functional perturbation theory (DFPT) used in the Quantum Espresso program.

3 Results and Discussion

3.1 Structural parameters

2D-MX_2 compounds can be synthesized as the honeycomb (H, trigonal prismatic), centered honeycomb (T, octahedral) and distorted honeycomb (T') structures. In this paper, the stable structures in the H configuration are considered. The general crystal structure of the MX_2 sheets is shown in Fig. l. As given in Fig. 1, we realize the relaxation of lattice stresses and atomic forces in order to provide the geometrical parameters optimization.

The relaxed lattice constants, a(Å) bond lengths of M-X and X-X(Å) θ(deg), cohesive energies E_c(eV) and energy band gaps, E_g(eV) are presented in Table 1.

Table 1

Calculated lattice constants; bond lengths (d_{M-X} and dx-x); X-M-X bond angles (θ); cohesive energies (E_c (eV)) and energy band gaps (E_g) of selected stable, 2D single-layer MX_2 dichalcogenides

	a		**d_{M-X}**	**dx-x**	**θ**	**E_c**	**E_g**	
	(Å)	Exp(Å)	(Å)	(Å)	(deg)	(eV)	Cal (eV)	Exp (eV)
MoS_2	3.141	3.160 [18]	2.394	3.126	81.516	23.733	1.858 (K)	1.87[22] 1.89[23] 1.90[24]
WS_2	3.131	3.153[18]	2.388	3.121	81.618	23.569	1.974 (K)	1.98[25] 2.02[26] 2.05[27]
CrS_2	2.955		2.239	2.901	80.726	26.825	1.144 (K)	
NiS_2	3.445		2.254	2.124	56.205	205.323	0.114 (Γ-K)	
$MoSe_2$	3.262	3.299[19]	2.512	3.324	82.849	22.037	1.634 (K)	1.55[24] 1.57[28] 1.58[29]
WSe_2	3.252	3.282[20]	2.507	3.322	83.005	21.604	1.728 (K)	1.62[30] 1.64[31] 1.65[28]
$CrSe_2$	3.117		2.373	3.094	81.372	24.971	0.932 (K)	
$NiSe_2$	3.342		2.359	2.716	70.281	202.585	2.401 (Γ-K)	
$MoTe_2$	3.493	3.522[19]	2.699	3.588	83.317	19.940	1.225 (K)	1.10[32]
WTe_2	3.487	3.477[21]	2.699	3.594	83.502	19.192	1.204 (K)	1.15[33]
$CrTe_2$	3.395		2.584	3.369	81.350	22.742	0.658 (K)	
$NiTe_2$	3.593		2.521	2.865	69.255	135.070	0.495 (M-Γ)	

Among other TMDs, MoX_2 and WX_2 nanosheets have been much studied; both from experimental and theoretical points of view. The results show that the MoX2 and WX2 sheets have quite similar structural

parameters. These results are in good agreement with DFT calculations by Y. Ding [12], A. Kumar [34] and F. Zeng [35]. All the structural parameters calculated for all the analyzed compounds are nearly identical to the theoretical values reported by Ataca et.al. [10] at the LDA level of theory. For the same chalcogen, the largest lattice constants are obtained for NiX_2 monolayers, while the smallest ones are those of the CrX_2 sheets, due to the difference in metals radius. Although the structure seems to be independent of the metal element, monotonously increasing with atomic number of chalcogen as seen clearly.) Both the bond lengths dM-X and the in-sheet lattice constants increase as MS2 < MSe2 < MTe2 for the same metal atoms with increasing the chalcogen atomic radius.

The cohesive energies of selected monolayers are calculated accordingly $E_c[MX_2] = E_T[M] + 2E_T[X] - E_T[MX_2]$, where $E_T[M]$ and $E_T[X]$ are the total energies of the corresponding free M and X atoms, $E_T[MX_2]$ is the total energy of the MX_T. The results show that the calculated cohesive energies are all positive, which means the reaction is exothermic and MX_2 sheets are stable. Although the E_c values presented in our work are larger than those reported in the literature, the trend is preserved, the highest cohesive energy belongs to MS_2, and it decreases for MSe_2 with the lowest value for MTe_2.

3.2 Electronic properties

The electronic band structure has been calculated along the high symmetry points (M-Γ-K-M) in the Brillouin zone. Experimental values (and other theoretical values) are also given in Table 1 for comparison. The calculated band gaps of these stable 2D materials are shown in the last two columns of the Table 1. 2H phase of some monolayers (MoS_2, $MoSe_2$, $MoTe_2$, WS_2, WSe_2, WTe_2) have direct band gaps in according to photoluminescence spectroscopy so, we also reproduce these properties with the LDA calculations. We find that direct band gaps for CrS_2, $CrSe_2$, and $CrTe_2$ materials with gaps of 1.144, 0.932, and 0.658 eV respectively. All NiX_2 dichalcogenides have indirect gaps in the range of 0.114-2.40l eV. CrX_2, MoX_2 and WX_2 sheets are nonmagnetic materials in H structure. Nevertheles, NiX_2 sheets stable H structure in two dimensions and have metallic, except for some instability in verylong-wavelengths acoustical waves. Moreover, NiX_2 are known to have a freestanding and stable T structure with a slightly lower energy [36].

The band edges of all materials are situated at the high-symmetry K point, showing that these compounds might be interesting for optoelectronic applications. The 2D-TMDs have a band gap ranging from 0.1–2.4 eV which is in the visible and near infrared range of light. Furthermore, as we compare the dispersion curves along the M-Γ and K-Γ directions, we can see that the electronic structure is generally the same along these paths which correspond to different crystallographic directions. This means that these materials are highly isotropic, thus we would expect the same for their physical properties.

The partial charges for basis atoms in all monolayer structures have been also calculated using Bader's AIM method [37] and the results are given in Table 2. The chalcogen atoms (S, Se, and Te) attract electrons from transition metal atoms (Mo, W, and Cr) indicating stronger electronegativity. A transition metal atom with six valence electrons loses its charge and forms a strong intralayer covalent bond with a corresponding chalcogen atom with the same valence electrons. The charge transfer from transition metal atom outer

shells to Te is smaller than the amount transferred to S or Se sites, as expected. The results of NiX_2 dichalcogenides also depict small charge transfer from Ni sites to S or Se regions, which indicates a covalent-type bonding between these atoms. On the other hand, the electronegativity difference between Ni and Te atoms becomes smaller, leading to a rather smaller amount of charge transfer from Te to Ni sites.

Table 2
Calculated charges by Bader analysis of 2D single-layer MX_2 dichalcogenides

	MoS_2		$MoSe_2$		$MoTe_2$
Mo	4.440	Mo	4.711	Mo	5.181
S	6.781	Se	6.639	Te	6.413
S	6.779	Se	6.650	Te	6.406
	WS_2		WSe_2		WTe_2
W	4.052	W	4.445	W	5.051
S	6.949	Se	6.740	Te	6.491
S	6.998	Se	6.814	Te	6.457
	CrS_2		$CrSe_2$		$CrTe_2$
Cr	4.603	Cr	4.874	Cr	5.218
S	6.705	Se	6.571	Te	6.389
S	6.692	Se	6.555	Te	6.392
	NiS_2		$NiSe_2$		$NiTe_2$
Ni	9.435	Ni	9.669	Ni	10.076
S	6.237	Se	6.186	Te	5.944
S	6.328	Se	6.145	Te	5.980

3.3 Vibrational properties

In practice, positive cohesive energy cannot determine whether the freestanding state of these structures will exist or not. For this purpose, the phonon dispersion calculations have been performed to check the dynamic stabilities of 2D MX_2 nanostructures. We have also calculated the phonon spectrum for further examination of the dynamical stabilities and vibrational spectrum of monolayers by using Density Functional Perturbation Methodology (DFPT) as implemented in QE [38]. Figure 3 shows the phonon dispersion of MX_2 monolayers through the high symmetry points. The unit cell of MX_2 structures has three basis atoms, so these unit cells include three acoustic (A) phonon branches and six optical (O) phonon branches. Also, there

is a linear relationship between transverse (TA) and longitudinal acoustic (LA) branches and the wave vector near point Γ. Furthermore, a characteristic feature of phonon dispersions for 2D materials has appeared, namely the quadratic out-of-plane acoustic (ZA) flexural mode. It is usually linear in 3D bulk materials because of strong interlayer interactions. Because the interlayer interactions are absent in 2D materials, it will cost less energy for the out-of-plane vibration and a quadratic dispersion will appear. This feature is closely related to the formation of the intrinsic ripples in 2D materials.

As seen in Fig. 3, phonons with longer wavelengths, i.e. around Γ in ZA mode have smaller frequencies or energies. This means this mode is more easily excited at low temperature and forms ripples which can be often observed in 2D materials at finite temperature. In the calculations, it is well reproduced quadratic behaviour of out-of-plane acoustic (ZA) mode and the linear behaviour of LA and TA modes near the zone center.

The analysis of the phonon branches shows that the maximum frequency values (ω_m) at the Γ point change as $\omega_{m,\mathrm{CrX_2}} > \omega_{m,\mathrm{MoX_2}} > \omega_{m,\mathrm{WX_2}} > \omega_{m,\mathrm{NiX_2}}$ for disulfides, diselenides and ditelluride monolayers mainly due to the bond stiffness, different average atomic masses of the monolayers. When the interatomic force constant becomes smaller (i.e. bond stiffness becomes weaker) and the atom mass becomes larger, the phonon frequencies decrease. The phonon dispersion curves of MX_2 compounds with M = Mo,W and Cr are in quite good agreement with the corresponding phonon curves reported by Ataca et al. [10]. Here the phonon dispersions for selected monolayers, except for $NiSe_2$, have real eigenfrequencies in the whole Brillouin zone, which is another indication of the stability of these dichalcogenides. Because of the large mass difference of the constiutent atoms of WS_2, it is observed a very large frequency gap between the acoustic and optical phonon branches in this compound. The large atomic weight difference between W and S base atoms also results in a very large phonon bandgap. The larger phonon gap in the compound is dependent upon the interatomic force and component atomic mass.

A remarkable aspect appears that the out of plane mode starts rippling for $NiSe_2$ monolayer and finally turns imaginary close to the K symmetry point of the BZ indicating the elastic nature of the material together with the lattice instability. This feature is similar to the $NiTe_2$ sheet. This mode carries most of the vibrational energy because of its lowest value among all phonon modes at the zone center. It has been noted in previous studies that the mode controls the properties and behaviour of graphene and all other 2D materials based devices [39]. Moreover, it can be seen that the ZA mode of $NiTe_2$ sheets has the maximum possibility to turn imaginary near the K-point of BZ. This can become unstable with lower force (external parameters) against long wavelength transversal waves. This instability, however, can be removed by defects such as ripples which do not allow these waves by limiting the size of sheets. Moreover, compared to CrX_2 monolayers, the acoustic branches of NiX_2 are less dispersive, owing to the weaker strength of Ni-X bonds than Cr-X bonds (X = S,Se,Te).

3.4 Debye temperatures

The average acoustic Debye temperature $\left(\varvec{\theta}_{\varvec{D}}\right)$ for a monolayer is calculated from the contributions of individual acoustic modes as:

$$\frac{1}{\varvec{\theta}_{\varvec{D}}^{3}}=\frac{1}{2}\left(\frac{1}{\varvec{\theta}_{\varvec{L}\varvec{A}}^{3}}+\frac{1}{\varvec{\theta}_{\varvec{T}\varvec{A}}^{3}}\right) \quad (1)$$

where $\varvec{\theta}_{\varvec{i}}$ $(\varvec{i}=\varvec{L}\varvec{A},\varvec{T}\varvec{A})$ is defined as

$$\varvec{\theta}_{\varvec{i}}=\frac{\hbar\varvec{\omega}_{\varvec{i},\varvec{m}\varvec{a}\varvec{x}}}{\varvec{k}_{\varvec{B}}} \quad (2)$$

with $\hbar$ Planck constant, $\varvec{\omega}_{\varvec{i},\varvec{m}\varvec{a}\varvec{x}}$ is the phonon frequency of the *i*.th acoustic mode at the zone boundary, and $\varvec{k}_{\varvec{B}}$ is the Boltzmann constant. The average atomic mass $\tilde{\varvec{M}}$, the mass ratio $\varvec{m}_{\varvec{M}}/\varvec{m}_{2\varvec{X}}$ and the calculated Debye temperature values of all the considered $\mathbf{MX}_2$ sheets are shown in Table 3. Debye temperatures of single layer MX_2 compounds have been treated in four groups as shown in the table. Debye temperatures $\varvec{\theta}_{\varvec{D}}$ for MoS_2, $MoSe_2$ and WS_2 are calculated as 291.19 K, 201.48 K, and 232.47 K, respectively, which agree with the 260–320 K estimated for MoS_2 from specific-heat measurement [40], 197.3± 66 K for $MoSe_2$ measured from photoconductivity measurements, 210 K for WS_2 obtained from Lindemann formula. The average atomic mass becomes an important quantity in the determination of the Debye temperatures of the monolayers. In Fig. 4, it is plotted the change in average atomic mass with Debye temperatures which is calculated for all groups. As expected, Debye temperatures vary with $\tilde{\varvec{M}}^{-1}$ approximately linearly. Accordingly, the highest $\varvec{\theta}_{\varvec{D}}$ of 338.20 K is obtained for CrS_2 structure corresponding to the minimum average atomic mass. On the other hand, we obtain 216.97 K for the Debye temperature of NiS_2 which has a similar mass with CrS_2.

Table 3

The average atomic mass ($\varvec{\tilde{M}}$), mass ratio ($\varvec{m}_{\varvec{M}}/\varvec{m}_{2\varvec{X}}$), and Debye temperature for MX_2 dichalcogenides

Structure	$\varvec{\tilde{M}}$ (amu)	$\varvec{m}_{\varvec{M}}/\varvec{m}_{2\varvec{X}}$	$\varvec{\theta}_{\varvec{D}}$ ($\varvec{K}$)
MoS_2	53.35	1.50	291.19
$MoSe_2$	84.62	0.61	201.48
$MoTe_2$	117.05	0.38	158.89
WS_2	82.66	2.87	232.47
WSe_2	113.92	1.16	189.15
WTe_2	146.35	0.72	148.43
CrS_2	38.71	0.81	338.20
$CrSe_2$	69.972	0.33	227.70
$CrTe_2$	102.40	0.20	169.10
NiS_2	40.94	0.92	216.97
$NiTe_2$	104.63	0.23	112.51

A similar trend is obtained for $CrTe_2$ and $NiTe_2$ with similar masses. It is found that the $\varvec{\theta}_{\varvec{D}}$ of $CrTe_2$ is about 56.6 (%33) larger than that of $NiTe_2$. These results are mainly due to the crucial effect of interatomic bonding in determining the Debye temperatures. The strong covalent bonding between Cr-S and Cr-Se in the third group compounds can result in relatively higher Debye temperatures as compared to the monolayers in the fourth one.

We obtain a graph $\varvec{\delta}\varvec{\theta}_{\varvec{D}}$ values versus to the inverse average atomic masses ($\varvec{\tilde{M}}^{-1}$) (Fig. 4). Where, $\varvec{\delta}$ calculated from $\varvec{\delta}^2 = \varvec{A}/\varvec{n}$ equation A is the unit cell area per number of atoms (n). $NiSe_2$ is only found as a dynamically unstable compound and the calculated Debye temperatures are influenced by the lattice constants and the average atomic mass. The obtained perfect linear $\varvec{\tilde{M}}^{-1}$ correlation in Fig. 4 indicates that these crystals could be quite anharmonic.

4 Conclusion

The electronic, structural, and dynamical properties of 12 different TMD monolayers are calculated by using first principles-based calculations. The MoX_2 and WX_2 monolayers have similar lattice parameters, electronic structures and as well as vibrational modes. Our band structure calculations indicate that MX_2 (M = Mo,W,Cr) group semiconducting sheets have direct band gaps at the K point following the order of $MS_2 > MSe_2 > MTe_2$. However, NiX_2 monolayers exhibit indirect gaps, while $NiSe_2$ and NiS_2 have the highest and the smallest band gaps among the studied compounds, respectively. We also obtain dynamical stabilities of the MX_2 sheets except for $NiSe_2$ with negative acoustic phonon modes near the K point. In addition, the effect of average atomic mass, the Debye temperature of dynamically stable monolayers is investigated. Our results reveal that the $\varvec{\theta}_{\varvec{D}}$ values of all these materials are inversely proportional to the average atomic mass. Meanwhile, the stronger covalent bonding between the transition metal and the chalcogen atoms gives rise to a higher Debye temperature of MX_2 sheets with similar atomic masses. This study points out the important role of the average atomic mass as well as the covalent bonding in determining the Debye temperatures of TMD monolayers and shows that TMDs have various of physical properties that could be useful for nano-electronics and optical devices.

Declarations

Author Contribution

A.Y.T. and N.B.Y. calculated the electronic and vibrational properties, plot all graphs, prepared Table 2 and Table 3 and wrote the main manuscript text. A.Y.T. also calculated the Debye temperatures.G.B.A. calculated the structural parameters, prepared Figure1, Table 1 and wrote the manuscript text.

References

1. Xu, M., Liang, T., Shi, M., Chen, H.: Graphene-like two-dimensional materials. Chem. Rev. **113**, 3766–3798 (2013)
2. Hayat, A.: Recent advances, properties, fabrication and opportunities in two-dimensional materials for their potential sustainable applications. Energy Storage Materials. **59**, 102780 (2023)
3. Bhimanapati, G.R.: Recent advances in two-dimensional materials beyond graphene. ACS Nano. **9**, 11509–11539 (2015)
4. Liu, P., Xiang, B.: 2D hetero-structures based on transition metal dichalcogenides: fabrication, properties and applications. Sci. Bull. **62**, 1148–1161 (2017)
5. Huang, X., Liu, C., Zhou, P.: 2D semiconductors for specific electronic applications: from device to system. npj 2D Materials and Applications. **6**, 51 (2022)
6. Choi, W., Choudhary, N., Han, G.H., Park, J., Akinwande, D., Lee, Y.H.: Recent development of two-dimensional transition metal dichalcogenides and their applications. Mater. Today. **20**, 116–130 (2017)
7. Jariwala, D., Sangwan, V.K., Lauhon, L.J., Marks, T.J., Hersam, M.C.: Emerging device applications for semiconducting two-dimensional transition metal dichalcogenides. ACS Nano. **8**, 1102–1120 (2014)

8. Wang, Q.H., Kalantar-Zadeh, K., Kis, A., Coleman, J.N., Strano, M.S.: Electronics and optoelectronics of two-dimensional transition metal dichalcigenides. Nat. Nanotechnol. **7**(11), 699–712 (2012)
9. Coleman, J.N.: Two-dimensional nanosheets produced by liquid exfoliation of layered materials. Science. **331**, 568–571 (2011)
10. Ataca, C., Şahin, H., Ciraci, S.: Stable, single-layer MX_2 transition-metal oxides and dichalcogenides in a honeycomb-like structure. J. Phys. Chem. C. **116**, 8983–8999 (2012)
11. Rasmussen, F.A., Thygesen, K.S.: Computational 2D materials database: Electronic structure of transition-metal dichalcogenides and oxides. J. Phys. Chem. C. **119**, 13169–13183 (2015)
12. Ding, Y., Wang, Y., Ni, J., Shi, L., Shi, S., Tang, W.: First principles study of structural, vibrational and electronic properties of graphene-like MX_2 (M = Mo, Nb, W, Ta; X = S, Se, Te) monolayers. Phys. B. **406**, 2254–2260 (2011)
13. Çakır, D., Peeters, F.M., Sevik, C.: Mechanical and thermal properties of h-MX_2 (M = Cr, Mo, W; X = O, S, Se, Te) monolayers: A comparative study. Appl. Phys. Lett. 104, 203110 (2014)
14. Hohenberg, P., Kohn, W.: Inhomogeneous electron Gas. Phys. Rev. B. **136**, 864–871 (1964)
15. Kohn, W., Sham, L.J.: Self-consistent equations including exchange and correlation Effects. Phys. Rev. **140**, A1133–A1138 (1965)
16. Giannozzi, P.: Quantum Espresso: a modular and open-source software project for quantum simulations of materials. J. Phys. : Condens. Matter. **21**, 395502 (2009)
17. Prasanjit, S., Manoj, K.H.: Local-density approximation for exchange energy functional in excited-state density functional theory. J. Phys. B: At. Mol. Opt. Phys. **38**, 3765–3777 (2005)
18. Luan, Q., Yang, C.L., Wang, M.S., Ma, X.G.: First-principles study on the electronic and optical properties of WS_2 and MoS_2 monolayers. Chin. J Phys. **55**, 1930–1937 (2017)
19. Babariya, B., Raval, D., Gupta, S.K., Gajjar, P.N.: Modulation of band gap and optical response of layered MoX_2 (X = S, Se, Te) for electronic and optoelectronic applications. Mater. Today Commun. **28**, 102614 (2021)
20. Li, H., Liu, S., Huang, S., Zhang, Q., Li, C., Liu, X., Meng, J., Tian, Y.: Metallic impurities induced electronic transport in WSe_2: First-principle calculations. Chem. Pys Lett. **658**, 83–87 (2016)
21. Gordon, R.A., Yang, D., Crozier, E.D., Jiang, D.T., Frindt, R.F.: Structures of exfoliated single layers of WS_2, MoS_2, and $MoSe_2$ in aqueous suspension. Phys. Rev. B. **65**, 125407 (2002)
22. Island, J.O., Kuc, A., Diependaal, E.H., Bratschitsch, R., van der Zant, H.S.J., Heine, T., Castellanos-Gomez, A.: Precise and reversible band gap tuning in single-layer $MoSe_2$ by uniaxial strain. Nanoscale. **8**, 2589–2593 (2016)
23. Mak, K.F., Lee, C., Hone, J., Shan, J., Heinz, T.F.: Atomically thin MoS ：A new direct gap semiconductor. Phys. Rev. Lett. **105**, 136805 (2010)
24. Tongay, S., Zhou, J., Ataca, C., Lo, K., Matthews, T.S., Li, J., Grossman, J.C., Wu, J.: Thermally driven crossover from indirect toward direct bandgap in 2D semiconductors: $MoSe_2$ versus MoS_2. Nano Lett. **12**, 5576–5580 (2012)

25. Zhao, W., Ghorannevis, Z., Chu, L., Toh, M., Kloc, C., Tan, P.H., Eda, G.: Evolution of electronic structure in atomically thin sheets of WS_2 and WSe_2. ACS Nano. **7**, 791–797 (2013)
26. Elias, A.L., Perea-Lopez, N., Castro-Beltran, A., Berkdemir, A., Feng, R., Lv, S., Long, A.D., Hayashi, T., Kim, Y.A., Endo, M., Gutierrez, H.R., Pradhan, N.R., Balicas, L., Mallouk, T.E., Lopez-Urias, F., Terrones, H., Terrones, M.: Controlled synthesis and transfer of large-area WS_2 sheets: From single layer to few layers. ACS Nano. **7**, 5235–5242 (2013)
27. Gutierrez, H.R., Perea-Lopez, N., Elias, A.L., Berkdemir, A., Wang, B., Lv, R., Lopez-Urias, F., Crespi, V.H., Terrones, H., Terrones, M.: Extraordinary room-temperature photoluminescence in triangular WS_2 monolayers. Nano Lett. **13**, 3447–3454 (2013)
28. Tonndorf, P., Schmidt, R., Böttger, P., Zhang, X., Börner, J., Liebig, A., Albrecht, M., Kloc, C., Gordan, O., Zahn, D.R.T., de Vasconcellos, S.M., Bratschitsch, R.: Photoluminescence emission and Raman response of monolayer MoS_2, $MoSe_2$, and WSe_2. Opt. Express. **21**, 4908–4916 (2013)
29. Zhang, Y., Chang, T.-R., Zhou, B., Cui, Y.-T., Yan, H., Liu, Z., Schmitt, F., Lee, J., Moore, R., Chen, Y., Lin, H., Jeng, H.-T., Mo, S.-K., Hussain, Z., Bansil, A., Shen, Z.-X.: Direct observation of the transition from indirect to direct bandgap in atomically thin epitaxial $MoSe_2$. Nat. Nanotechnol. **9**, 111–115 (2014)
30. Gusakova, J., Wang, X., Shiau, L.L., Krivosheeva, A., Shaposhnikov, V., Borisenko, V., Gusakov, V., Tay, B.K.: Electronic properties of bulk and monolayer TMDs: Theoretical study within DFT framework (GVJ-2e Method). Phys. Status Solidi A. **214**, 1700218 (2017)
31. Baugher, B., Churchill, H., Yang, Y., Jarillo-Herrero, P.: Optoelectronic devices based on electrically tunable p–n diodes in a monolayer dichalcogenide. Nat. Nanotechol. **9**, 262–267 (2014)
32. Ruppert, C., Aslan, O.B., Heinz, T.F.: Optical properties and band gap of single-and few-layer $MoTe_2$ crystals. Nano Lett. **14**, 6231–6236 (2014)
33. Kim, J.Y., Gelczuk, Ł., Polak, M.P., Hlushchenko, D., Morgan, D., Kudrawiec, R., Szlufarska, I.: Experimental and theoretical studies of native deep-level defects in transition metal dichalcogenides. npj 2D Mater. Appl. **6**, 75 (2022)
34. Kumar, A., Ahluwalia, P.K.: Electronic structure of transition metal dichalcogenides monolayers 1H-MX_2 (M = Mo,W; X = S,Se,Te) from ab-initio theory: new direct band gap semiconductors. Eur. Phys. J. B. **85**, 186 (2012)
35. Fan, Z., Wei-Bing, Z., Bi-Yu, T.: Electronic structures and elastic properties of monolayer and bilayer transition metal dichalcogenides MX_2 (M = Mo,W; X = O,S,Se,Te): A comparative first-principles study. Chin. Phys. B. **24**, 097103 (2015)
36. Ku, R., Yan, L., Xue, K., Zhang, J., Pang, K., Sha, M., Wang, B.-T., Jiang, Y., Zhou, L., Li, W.: NiX_2 (X = S,Se, and Te) Monolayers: Promising Anodes in Li/Na-Ion Batteries and Superconductors. J. Phys. Chem. C. **126**, 6925–6933 (2022)
37. Bader, R.F.W.: Atoms in Molecules: A Quantum Theory. Oxford University Press, Oxford (1990)
38. Giannozzi, P., Baroni, S.: Handbook of Materials Modeling, pp. 195–214. Springer (2005)
39. Ares, P., Novoselov, K.S.: Recent advances in graphene and other 2D materials. Nano Mater. Sci. **4**, 3–9 (2022)

40. Peng, B., Zhang, H., Shao, H., Xu, Y., Zhang, X., Zhu, H.: Thermal conductivity of monolayer MoS_2, $MoSe_2$, and WS_2: interplay of mass effect, interatomic bonding and anharmonicity. RSC Adv. **6**, 5767–5773 (2016)

Figures

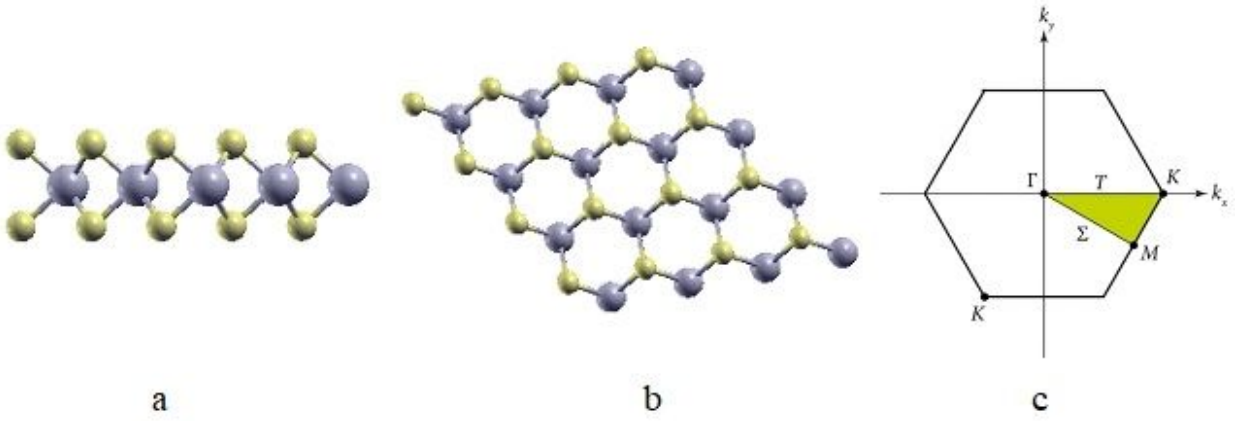


Figure 1

a The side and **b** top view of MX_2 monolayers in the 2H phase, where grey and yellow balls represent M and X atoms, respectively. **c** The first Brillouin zone and the high symmetry points of two-dimensional honeycomb lattice

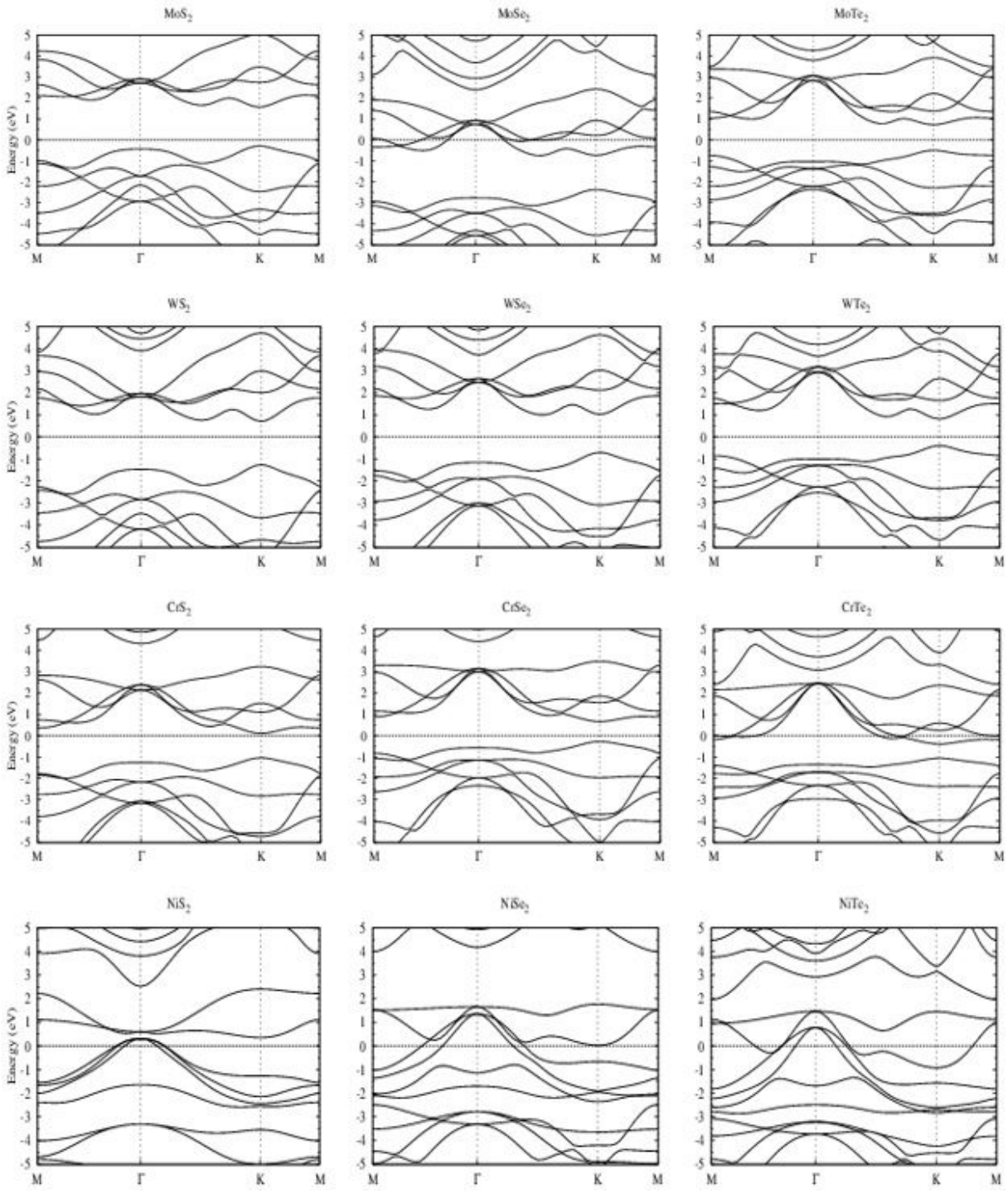


Figure 2

The band structures for monolayer TMDs calculated using LDA. The Fermi level is set at $E = 0.0$ eV

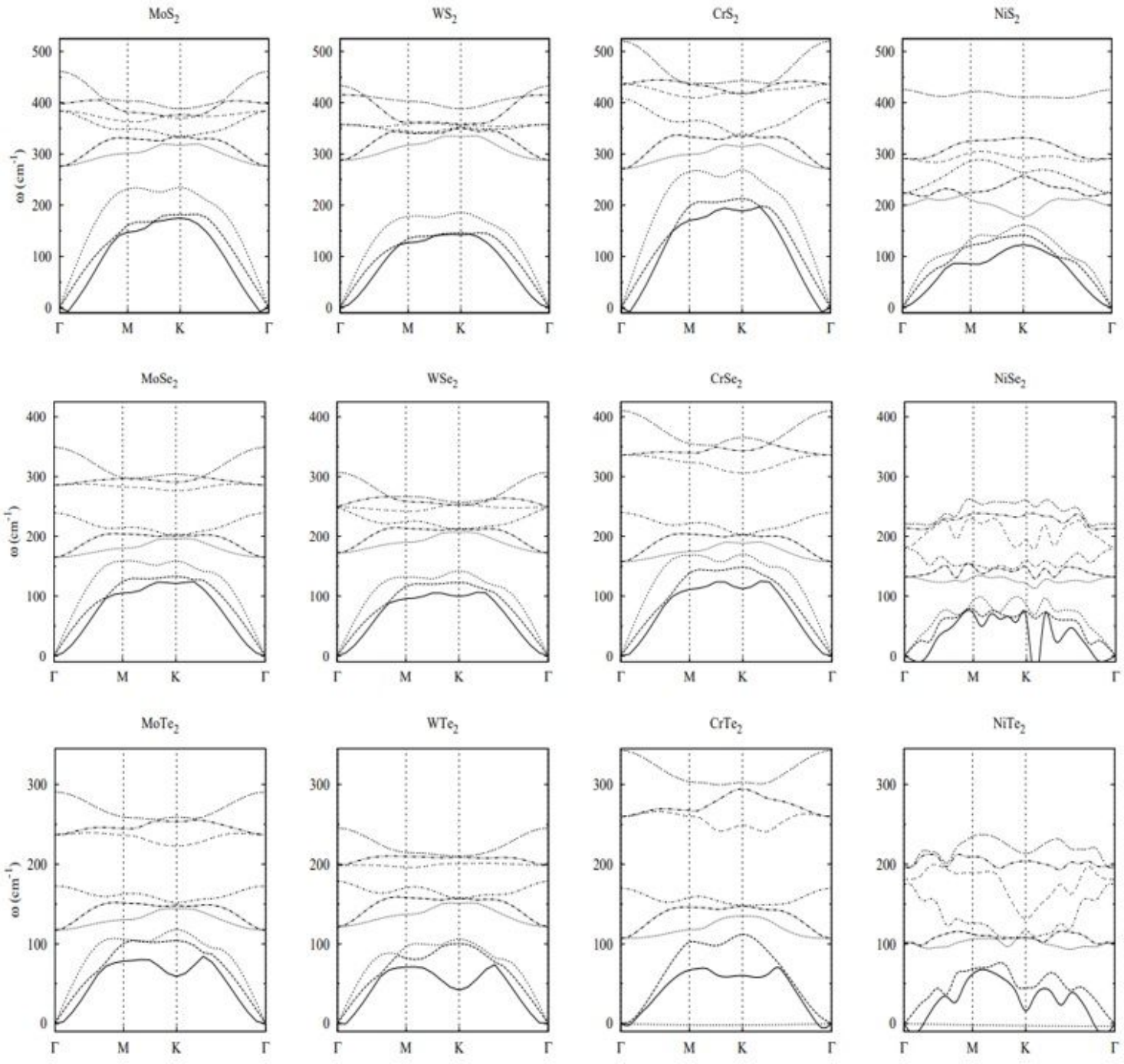


Figure 3

e calculated phonon dispersion curves for MX_2 monolayers along high symmetry points Γ-M-K-Γ

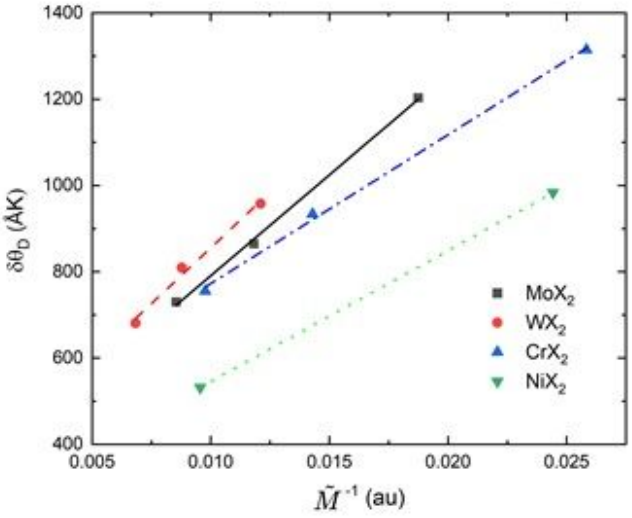


Figure 4

The calculated $\delta\theta_D$ values versus $\tilde{M}^{-1}$. X represents the chalcogen atoms (S, Se, and Te). NiSe2, found as dynamically unstable compound is not included in the calculations. The dashed lines show the linear fitting values

Supplementary Files

This is a list of supplementary files associated with this preprint. Click to download.

- Table1.png
- Table2.png
- Table3.png